



HAL
open science

Multilayer phoswich scintillators for neutron / gamma discrimination

Romain Coulon, Vladimir Kondrasovs, Quentin Lecomte, Jonathan Nicolas Dumazert

► **To cite this version:**

Romain Coulon, Vladimir Kondrasovs, Quentin Lecomte, Jonathan Nicolas Dumazert. Multilayer phoswich scintillators for neutron / gamma discrimination. Radiation Measurements, 2018, 117, pp.57 - 62. 10.1016/j.radmeas.2018.07.011 . cea-01915979

HAL Id: cea-01915979

<https://cea.hal.science/cea-01915979>

Submitted on 7 Jun 2022

HAL is a multi-disciplinary open access archive for the deposit and dissemination of scientific research documents, whether they are published or not. The documents may come from teaching and research institutions in France or abroad, or from public or private research centers.

L'archive ouverte pluridisciplinaire **HAL**, est destinée au dépôt et à la diffusion de documents scientifiques de niveau recherche, publiés ou non, émanant des établissements d'enseignement et de recherche français ou étrangers, des laboratoires publics ou privés.

Multilayer phoswich scintillators for neutron / gamma discrimination

R. Coulon¹, V. Kondrasovs¹, Quentin Lecomte¹, Jonathan Dumazert¹

1. CEA, LIST, Laboratoire Capteurs et Architectures Electroniques, F-91191 Gif-sur-Yvette, France.

Abstract– A multi-layer phoswich scintillator is studied by the CEA LIST to address the issue of fast neutron detection. In the proposed approach the neutron are discriminated from gamma background using recoil-particle range differentiation. A simulation study of such a system has been realized using MCNPX Monte-Carlo transport code and a specific program has been developed to extract and process the PTRAC output files. It has been observed a strong anisotropic effect when thin layers are used (<1 mm) and two antagonist effects (neutron induced signal vs. gamma induced signal) which allow us to define the optimal range of operability around 300 μm. Despite of a poor discrimination strength compared to conventional PSD scintillators, the multilayer phoswich can find its interest for neutron source localization thanks to its high direction dependence with neutron angle of incidence.

I. INTRODUCTION

NEUTRON measurement is a major issue in many applications as for security (radiological treat), fuel manufacturing and processing, Nuclear Power Plant safety and operating. Thermal neutrons are efficiently detected using helium 3 gas detectors which exhibit an excellent discrimination between neutron and gamma events. In a context of shortage in helium 3, alternative solutions have been developed using thermal neutron capture into Boron, Lithium or Gadolinium [1-6]. These systems require the implementation of moderator whereas fast neutron detectors enable neutron from Special Nuclear Materials (SNM) to be directly detected using light ion recoil consecutively to elastic scattering (n, n'). Fast neutron based detectors are therefore more suitable for compact systems or to be used in cluster for implementing coincidence techniques [7, 8]. The discrimination mechanism exploits energy transfer between two triplet state called intersystem crossings. This Triplet-Triplet Annihilation (TTA) is allowed only when a sufficient energy density is achieved in a given polymer matrix [9,10]. Indeed, the density of energy released by recoil protons from neutron elastic scattering is superior to the energy density of recoil electrons from gamma-rays Compton scattering. As a consequence, gamma rays will induced fluorescence (direct radiative transition from the first excited singlet state to the fundamental state) whereas neutron particles will produced delayed fluorescence (due to delay time in the triplet state before TTA) in some polymers and for a given deposited energy. The impulse response is therefore dissociated between neutron and gamma rays thanks to the implementation of Pulse Shape Discrimination PSD technique in the Digital Signal Processing DSP of the system. This approach is known to be very efficient in liquid state scintillators where intermolecular energy transfer is fostered [11, 12]. However, liquid scintillators have to be carefully encapsulated due to their

toxicity, their low flash point and their oxygen adsorption damaging scintillator performances over the time. Therefore plastic scintillators are more suited for handle and long term of use and some recent works show promising results [13, 14].

Another discrimination technique has been proposed by M.A. Kovash for solid state plastic scintillator [15]. Recoil protons and electrons have the property to possess distinct path lengths for a given kinetic energy. As presented in the fig. 1, the range of recoil electrons from gamma-rays is two orders of magnitude higher than the range of recoil protons from neutrons for a given energy. The system proposed by the authors of [15] is composed of thin layers (100 μm) optically isolated to each other and associated to a coincidence electronics. Pulse detected in coincidence between adjacent layers is considered as gamma-rays and are then rejected.

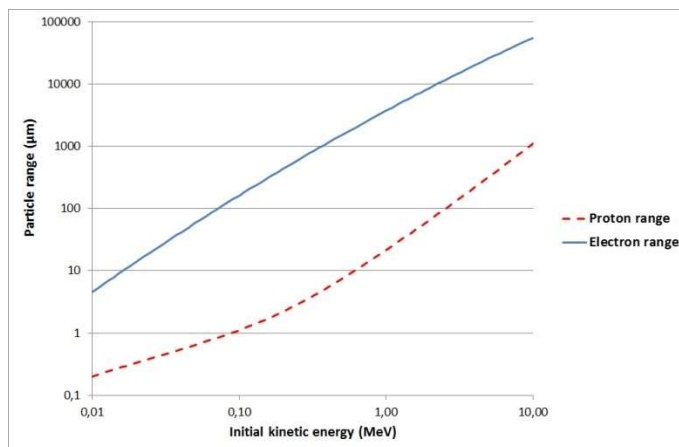


Fig.1. Range of electrons calculated by Katz and Penfold formula [16] and protons calculated by SRIM [17].

The CEA LIST has patented and implemented a layered scintillator in an alternative configuration where the layers are non-optically insulated, composed of a polymer matrix doped with different fluorophores (inducing fast and slow scintillators) and associated with PSD electronics [18]. On the first hand, output pulses resulting from proton recoils comes from single layer interactions and they can be shape fast or slow (neutron interaction). On the other hand, a mixed pulse shape is observed for recoil electrons slowing-down through adjacent layers (gamma interaction). The fig. 2 illustrates the concept of the system.

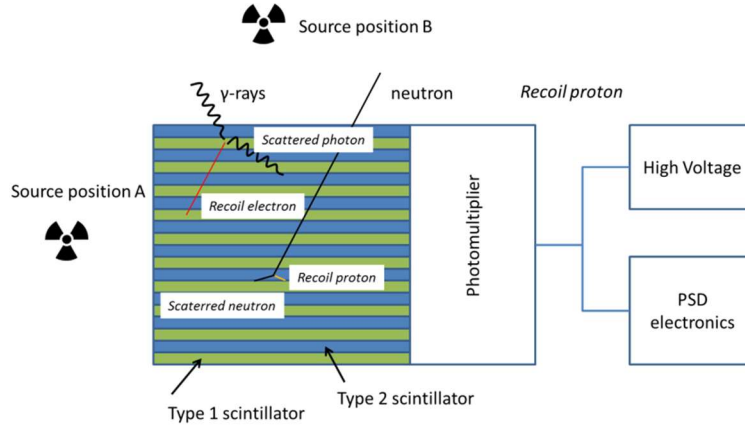


Fig.2. Principle of the multilayer scintillator.

The multilayer phoswich scintillator has been studied by particle transport simulation. This study is detailed in following sections.

II. MATERIAL AND METHOD

The simulation study has been realized using MCNPX Monte-Carlo particle transport code [19]. The geometry is composed of twenty alternating layers (25 x 25 mm). Source particles (neutron or gamma) are generated next to the scintillator and data associated with recoil particle collisions are recorded into the MCNPX PTRAC file.

1. Interaction models in γ/e^- and n/p modes

We consider first the formatting of electron broken line path in the γ/e^- mode. Let N_h^δ the number of the collision δ , $1 \leq \delta \leq N_h$ associated with the history number h . PTRAC file is processed to extract in each history h :

- the coordinate X_h^δ of δ collisions,

$$\forall \delta \in [1; N_h], X_h^\delta = \{x_{h,1}^\delta; y_{h,1}^\delta; z_{h,1}^\delta\} \quad (1)$$

- the final position of delta-rays coming from the δ collisions,

$$\forall \delta \in [1; N_h], Y_h^\delta = \{x_{h,2}^\delta; y_{h,2}^\delta; z_{h,2}^\delta\} \quad (2)$$

- the initial kinetic energy $E_{h,0}$ of the recoil electron coming from Compton scattering,
- the kinetic energy $E_{h,2}^\delta$ of each delta electrons,
- the cell number C_h^δ in which δ collision has occurred.

MCNP code ensures electron transport up to 1 keV. As we know, the electron collision threshold is close below 1 keV, we can then consider that ionization and excitation induced by the recoil electron are described along the track path described here. At the end of the electron slowing down, the deposited energy $E_{h,2}^\delta$ is spread along the delta electron path in one hand. On the other hand, the energy $E_{h,1}^\delta$ is released in the path of the primary recoil electron between two collisions δ and $\delta + 1$ as described in the following equations where d_h^δ is the distance path between collisions:

$$\forall \delta \in [1, N_h - 1],$$

$$d_h^\delta = \sqrt{(x_{h,1}^{\delta+1} - x_{h,1}^\delta)^2 + (y_{h,1}^{\delta+1} - y_{h,1}^\delta)^2 + (z_{h,1}^{\delta+1} - z_{h,1}^\delta)^2} \quad (3)$$

$$E_{h,1}^\delta = \frac{(E_{h,0} - \sum_{\omega=1}^\delta E_{h,2}^\omega) d_h^\delta}{\sum_{\omega=1}^{\delta-1} d_h^\omega} \quad (4)$$

Let $\rho = \{S_1; S_2\}$ the scintillator type numbers (fast / slow pulse time constant), quantities of deposited energy $E_{h,\rho}^{e^-}$ in each scintillator type ρ is calculated such as:

$$\forall \delta \in [1, N_h - 1] \ \& \ \forall \rho \in [S_1; S_2],$$

$$E_{h,\rho}^{e^-} = \sum_{\delta, C_h^\delta \in \rho} E_{h,1}^\delta + E_{h,2}^\delta \quad (5)$$

In n/p mode, the neutron cross-section library ENDF B-VI and the proton cross-section library la150h are used. Protons are decelerated in straight line mainly by Coulomb force and all the energy E_h is considered to be released along its path. In this mode, delta electron production is considered as neglected ($N_h = 1$), then PTRAC processing allow us to calculate directly released energies $E_{h,\rho}^p$ into the two types of scintillator.

$$\forall \rho \in [S_1; S_2],$$

$$E_{h,\rho}^p = \sum_{\delta, C_h^\delta \in \rho} E_h \quad (6)$$

Figs. 3 and 4 show an example of a recoil electron and a recoil proton path.

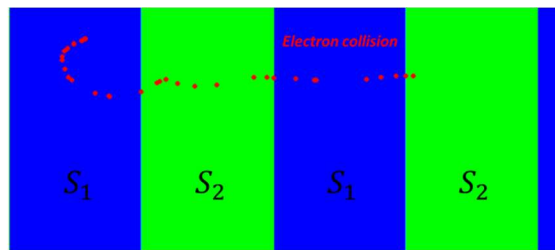


Fig.3. Scheme of a recoil electron path into the multilayer system.

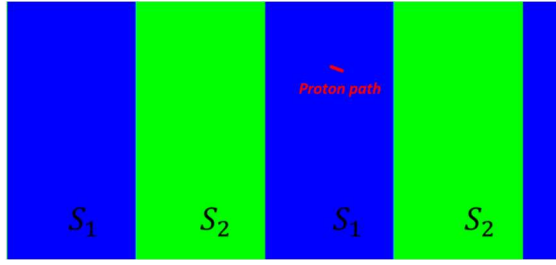


Fig.4. Scheme of a recoil proton path into the multilayer system.

2. Model of the scintillation

A particularity of scintillation is the quenching effect in which the light yield L is reduced as a function of the type of polymer and the type of particles (*cf.* the semi-empirical Birks formula [20]). The quenching phenomenon is increase for hadronic recoil particles compared to leptonic ones, respectively protons and electrons in our case. The reduced energy \dot{E}_h^p in MeVee is calculated for proton particles using the empirical relation proposed by [21] such as:

$$\dot{E}_h^p = -0.0685 + 0.223E_h^p \quad (7)$$

Scintillation is a quantum phenomenon where the expected number of photon quanta is proportional to the deposited energy from charges particles. As quanta are uncorrelated together, the effective number of quanta governing the scintillation pulse area (and amplitude) takes its value in Poisson distribution. Measured energies \ddot{E}_h^p and $\ddot{E}_h^{e^-}$ associated to each individual interaction, are obtained by sampling into a Poisson distribution \mathcal{P} where \dot{E}_h^p and $E_h^{e^-}$ are expected deposited energy values.

$\forall \rho \in [S_1; S_2]$,

$$\ddot{E}_{h,\rho}^p \sim \frac{\mathcal{P}(L_\rho \dot{E}_{h,\rho}^p)}{L_\rho} \quad (8)$$

$$\ddot{E}_{h,\rho}^{e^-} \sim \frac{\mathcal{P}(L_\rho E_{h,\rho}^{e^-})}{L_\rho} \quad (9)$$

3. Pulse shape discrimination matrix calculation

The PSD matrix called M is an $n \times n$ matrix, where rows correspond to energies measured in the type S_1 scintillator and columns correspond to energies measured in the type S_2 scintillator. Let $e_{\rho,i}$ the energy vector, ρ the scintillator type S_1 or S_2 , and ΔE the energy bins.

$$\forall i \in [1; n], \quad e_{\rho,i} = \{\Delta E; 2\Delta E; \dots; i\Delta E; \dots; n\Delta E\} \quad (10)$$

The pairs $\ddot{E}_{h,\rho}^\zeta = \{\ddot{E}_{h,S_1}^\zeta; \ddot{E}_{h,S_2}^\zeta\}$, where the particle type ζ can be p or e^- depends on the interaction mode n/p or γ/e^- , are

digitized such as:

$$\forall h \ \& \ \forall \rho \in [S_1; S_2],$$

$$\varepsilon_{\rho,h} = \operatorname{argmin}_i \{\ddot{E}_{h,\rho}^\zeta > e_{\rho,i}\} \quad (11)$$

$$M_{\varepsilon_{S_1,h}, \varepsilon_{S_2,h}}^\zeta := M_{\varepsilon_{S_1,h}, \varepsilon_{S_2,h}}^\zeta + 1 \quad (12)$$

Fig. 5 illustrates the theoretical composition of the discrimination matrix. Three areas can be distinguished:

- a neutron interaction area where recoil protons have released their kinetic energies in a type A scintillation layer (I),
- a gamma interaction area where recoil electrons have released their kinetic energies in both types of scintillation layer (II),
- a neutron interaction area where recoil protons have released their kinetic energies in a type B scintillation layer (III),

If the two types of layer are with the same thickness, we can predict that the PSD matrix will presents a diagonal line of symmetry.

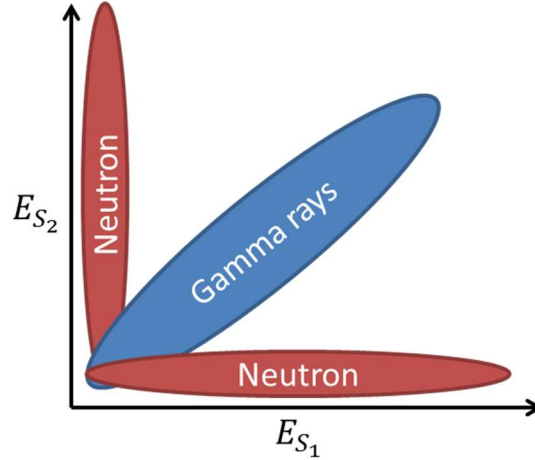


Fig.5. Theoretical composition of the discrimination matrix.

4. Figure of merit & intrinsic neutron efficiency

The discrimination strength of the system is estimated using a Figure Of Merit FOM_i defined as the distance between mean energy of neutron \bar{E}_i^p and gamma $\bar{E}_i^{e^-}$ lobes divided by the sum of associated standard deviations $\sigma(E_i^{e^-})$ and $\sigma(E_i^p)$ at a given energy e_i .

$$FOM_i = \frac{\bar{E}_i^{e^-} - \bar{E}_i^p}{\sigma(E_i^{e^-}) + \sigma(E_i^p)} \quad (13)$$

As a FOM value above the unit allows the system to be considered as a potential neutron counter [22], the intrinsic neutron efficiency η (i.e. *proton efficiency*) is calculated as the sum of neutron counted above an energy threshold α corresponding to the minimum energy ensuring discrimination ($FOM > 1$).

$$\alpha = \underset{i, 1 \leq i \leq n}{\operatorname{argmin}}(FOM_i > 1) \quad (14)$$

$$\eta = \frac{\sum_{u=\alpha}^n \sum_{v=\alpha}^n M_{u,v}^p}{h} \quad (15)$$

III. RESULTS

The simulation study has been conducted in order to determine the behavior of layered phoswich scintillator as a function of the layer thickness δ . PSD matrixes have been calculated for different values of layer thickness such as: $\delta = \{0.025; 0.050; 0.100; 0.300; 0.500; 1.000\}$ mm for both source positions A and B (cf. fig. 2). The energy binning ΔE has been taken equal to 5 keVee. The figs. 6 and 7 show matrixes obtained with gamma and neutron irradiations. The shapes are in accordance with the expected phenomena introduced in the fig. 5 with a concentration of gamma events in the central part of the PSD matrix whereas neutron events are mainly located along edges of the PSD matrix.

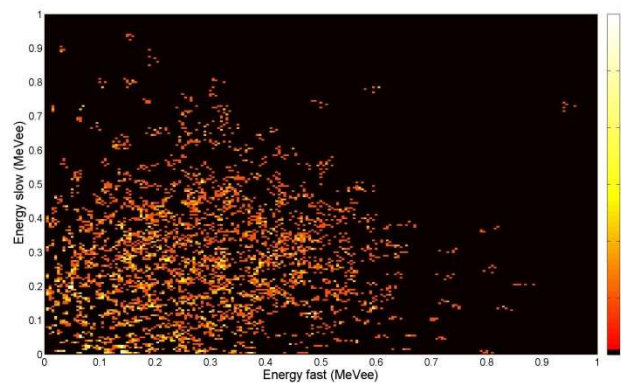


Fig. 6. PSD matrix obtained by simulation of a ^{60}Co source located in position B for a layer thickness equal to 300 μm .

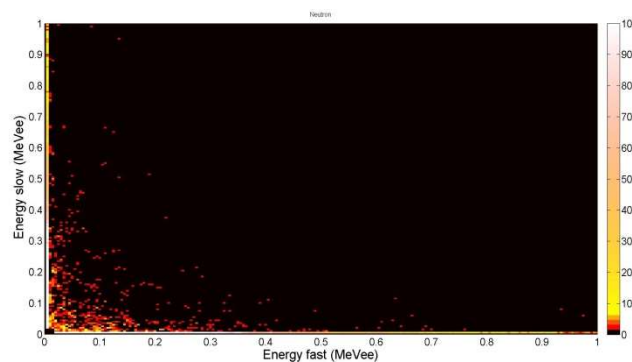


Fig. 7. PSD matrix obtained by simulation of a ^{252}Cf source located in position B for a layer thickness equal to 300 μm .

Figures of merits FOM calculated as a function of the deposited electron equivalent energy e are presented in figs. 8-10 for thickness values $\delta = \{0.025; 0.300; 1.000\}$ mm layer thickness. It can be observed that the discriminability strongly depends on the layer thickness and the relative position between scintillator and sources. When layers are too thin, as seen in fig. 8 (25 μm), high energy protons (>650 keVee) go through more than one layer. Moreover the anisotropy is maximized in this particular case, where discrimination is enabled between 250 and 650 keVee in position B, whereas discrimination is completely impossible in position A. More the layers grow in thickness, more the discrimination strength becomes flat as a function of the energy, and more the isotropic behavior is increased. It can be observed in fig. 10, that FOM values between 100 keVee and 1 MeVee and for a layer thickness equal to 1 mm are constant ($FOM \approx 1.5$) and identical for both positions A and B. The homogeneity behavior achieved for $\delta = 1$ mm against energy range and source position is balanced by low discrimination power while a more efficient discrimination is enable as seen for $\delta = 300$ μm ($FOM > 2$ in position B and for $e \in [0.4; 1]$ MeVee) if a part of inhomogeneity is accepted (*cf.* fig. 9). We can conclude that it will be not probably possible to maintain as well discrimination capability and homogeneity (isotropy and energy stability).

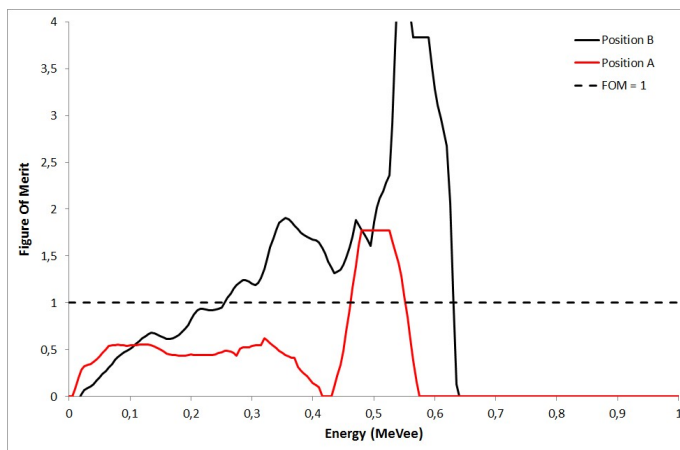


Fig. 8. FOM estimation as a function of the deposited energy e for a layer thickness equal to 25 μm ($^{60}\text{Co} + ^{252}\text{Cf}$).

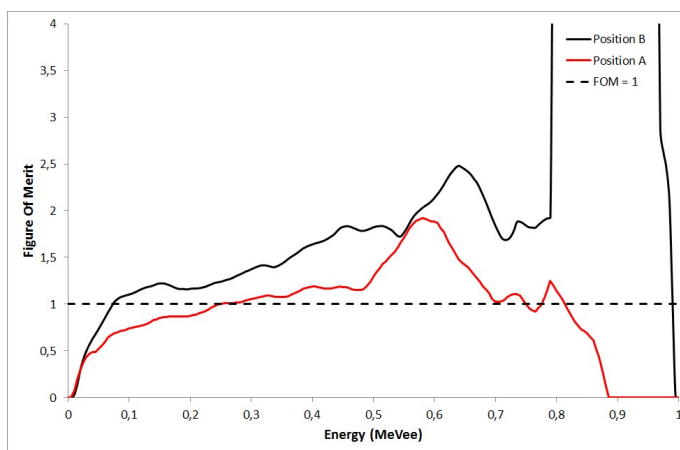


Fig. 9. FOM estimation as a function of the deposited energy e for a layer thickness equal to 300 μm ($^{60}\text{Co} + ^{252}\text{Cf}$).

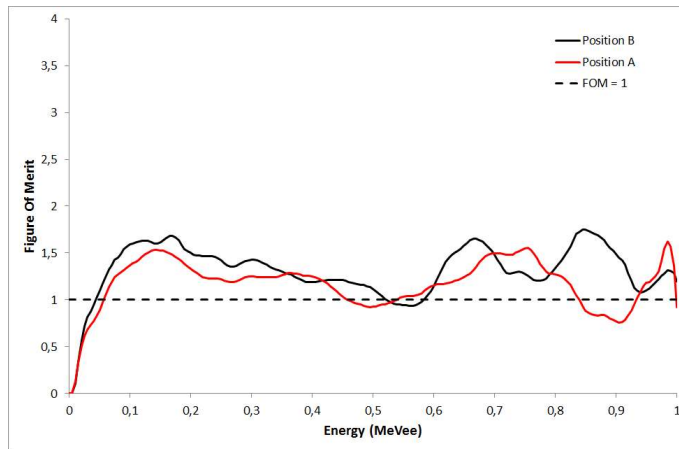


Fig. 10. *FOM* estimation as a function of the deposited energy e for a layer thickness equal to 1 mm ($^{60}\text{Co} + ^{252}\text{Cf}$).

The discrimination principle deals with two antagonistic effects illustrated in Fig. 11. The elastic scattering (n,n') pushes the nucleus of an hydrogen atom behind the incident neutron direction. In thin layer case, neutrons coming from the position B are able to produce a large amount of recoil protons crossing through adjacent layers. As the electrons from Compton scattering are less directionally depends with regards to gamma rays incident angle, the number of mixture pulses induced by recoil electrons is large and independent from source position. When layer thickness is increased, the number of proton depositing its kinetic energy in only one layer increases. Discrimination is therefore fostered but the number of recoil electrons from photons interacting in one layer will also increases damaging discrimination.

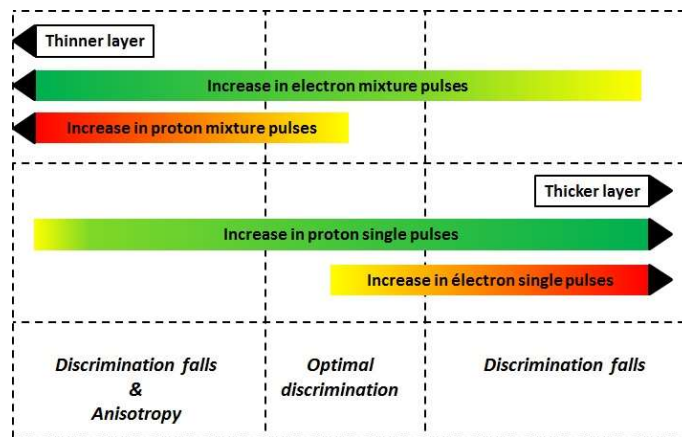


Fig. 11. Scheme of the discrimination technique principle.

The proton recoil signal induced by a fission source is comprised between 0 to 0.8 MeV but quenching effects reduce the measured energy in the energy range 0 to 0.4 MeVee. The energy threshold α has to be set as low as possible to maximize the proton efficiency η (i.e. intrinsic efficiency). Fig. 12 shows α threshold values ensuring a FOM value above the unit as a function of the layer thickness. The threshold allowing discrimination is reduced with the decrease of layer thickness.

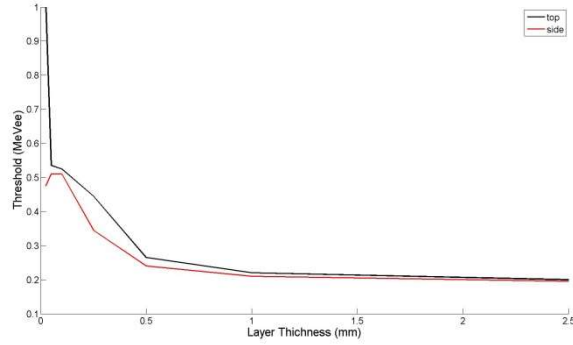


Fig. 12. Electron equivalent energy threshold α as a function of layer thickness δ ($^{60}\text{Co} + ^{252}\text{Cf}$).

The proton efficiency η (*i.e.* intrinsic neutron efficiency) has been calculated with α estimations as a function of layer thickness for both source positions (average). Fig. 13 shows proton efficiencies estimation using ^{137}Cs interference source and ^{252}Cf as neutron source. According to this simulation study, we can conclude that proton efficiency is maximized for a layer thickness equal to 300 μm . In this case, an anisotropic effect is observed above 0.8 MeVee (fig. 9) but only concerns a small amount of recoil protons from fission neutrons. Proton efficiency about 0.2 % could be achieved by the proposed techniques.

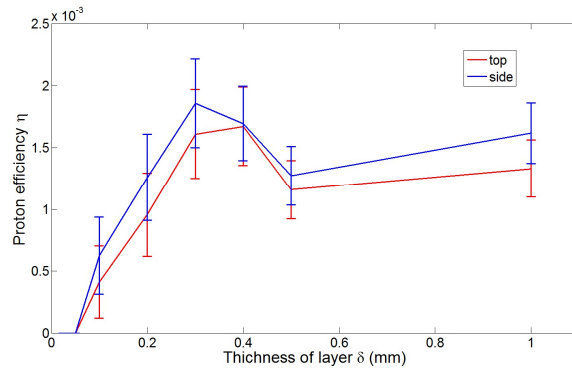


Fig. 13. Proton efficiency η as a function of the layer thickness δ ($^{137}\text{Cs} + ^{252}\text{Cf}$).

IV. DISCUSSION

An interest in such approach could consist in neutron source localization using the anisotropic properties of the scintillator. For instance, a multilayered phoswich can be installed on a rotor fixed on a mobile robot as inspired by [23].

V. CONCLUSION

A model allowing simulating neutron measurement of a multilayer phoswich scintillator has been developed. The behavior of the system as a function of the layer thickness has been investigated and strong incidence angle dependence has been predicted especially when layer are below 100 μm . Moreover, the optimum discrimination efficiency has been estimated at 300 μm but the system still shows a low discrimination strength due to the high dispersion of gamma event into PSD matrixes whatever layer thickness or incident energy are. A localization device is under study using this innovative component as a direction sensitive neutron detector.

REFERENCES

- [1] Kouzes, R. T., *et al.*, *Nuclear Instruments and Methods in Physics Research A*, 623:3 (2010) 1035–1045.
- [2] Lacy, J. L., *et al.*, *Nuclear Instruments and Methods in Physics Research A*, 652:1 (2011) 359–363.
- [3] Bertrand, G. H. V., *et al.*, *Journal of Materials Chemistry C*, 3 (2015) 6006–6011.
- [4] Dumazert, J., *et al.*, *Nuclear Instruments and Methods in Physics Research Section A*, 828 (2016) 181–190.
- [5] Dumazert, J., *et al.*, *IEEE Transactions on Nuclear Science*, 63:3 (2016) 1551–1564.
- [6] Normand, S., *et al.*, *Nuclear Instruments and Methods in Physics Research A*, 484 (2002) 342–350.
- [7] Pozzi S.A., Oberer R.B., and Chiang L.G., *ORNL Report*, ORNL/TM-2000/295 (2000).
- [8] Deyglun, C., *et al.*, *In Proceeding of ANIMMA* (2013).
- [9] Birks J.B., *The Theory and Practice of Scintillation Counting*, edited by Pergamon Press, 27 (1964) 219–227.
- [10] Brooks, F. D., *Nuclear Instruments and Methods*, 162 (1979) 477–505.
- [11] Hamel, M., *et al.*, *Nuclear Instruments and Methods in Physics Research A*, 602 (2009) 425–431.
- [12] Montbarbon, E., *et al.*, *Chemistry - A European Journal*, 22:34 (2016) 12074–12080.
- [13] Zaitseva, N., *et al.*, *Nuclear Instruments and Methods in Physics Research A*, 668 (2012) 88–93.
- [14] Blanc, P., *et al.*, *Nuclear Instruments and Methods in Physics Research A*, 750 (2014) 1–11.
- [15] Kovash, M. A., *et al.*, *In Proceeding of ANIMMA* (2011) 2–4.
- [16] Katz, L., & Penfold, A. S., *Reviews of Modern Physics*, 24:1 (1952) 28–44.
- [17] Ziegler, J. F., *et al.*, *Nuclear Instruments and Methods in Physics Research B*, 268 (2010) 1818–1823.
- [18] Kondrasovs, V. *et al.*, US Patent US20150346362 A1 (issued December 3, 2015).
- [19] Pelowitz, D.B., *LANL Report*, LA-CP-11-00438 (2011).
- [20] Tretyak, V. I., *Astroparticle Physics*, 33 (2010) 40–53.
- [21] Marseguerra, M., *et al.*, *Nuclear Instruments and Methods in Physics Research B*, 213 (2004) 289–293.
- [22] Marisaldi, M., *et al.*, *IEEE Transactions on Nuclear Science*, 51:4 (2004) 1916–1922.
- [23] Miller, A., Machrafi, R., & Mohany, *Radiation Measurements*, 72 (2015) 53–59.